CSIRO PUBLISHING

Australian Journal of Physics

Volume 50, 1997

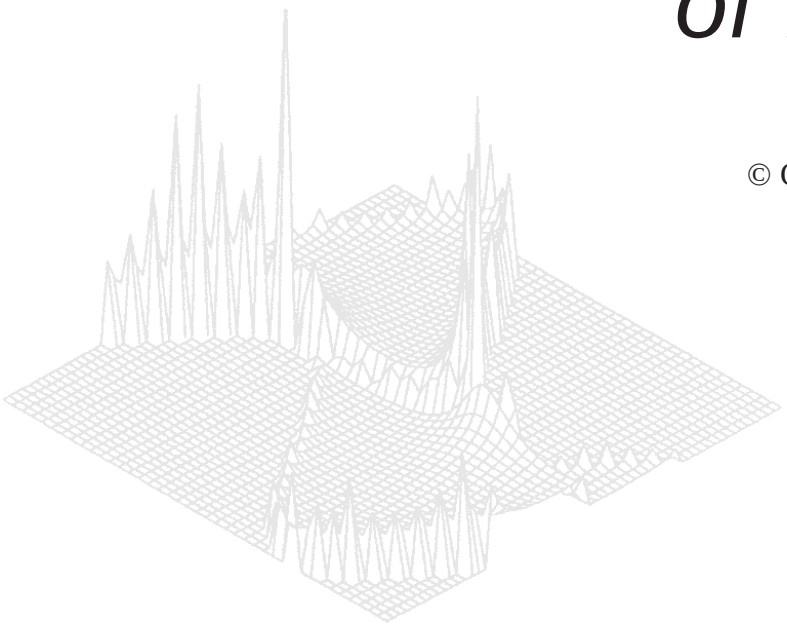

A journal for the publication of
original research in all branches of physics

www.publish.csiro.au/journals/ajp

All enquiries and manuscripts should be directed to
Australian Journal of Physics
CSIRO PUBLISHING
PO Box 1139 (150 Oxford St)
Collingwood Telephone: 61 3 9662 7626
Vic. 3066 Facsimile: 61 3 9662 7611
Australia Email: peter.robertson@publish.csiro.au

Published by **CSIRO** PUBLISHING
for CSIRO Australia and
the Australian Academy of Science

Aust. J. Phys., 1997, **50**, 245–54

Signatures of Medium Effects on NN Interactions in Proton Scattering from Nuclei*

K. Amos, P. J. Dortmans and S. Karataglidis

School of Physics, University of Melbourne,
Parkville, Vic. 3052, Australia.

Abstract

Effective two nucleon (NN) interactions in the nuclear medium have been defined from an accurate mapping of NN g matrices obtained by solving the Brueckner–Bethe–Goldstone (BBG) equations for infinite nuclear matter. Those effective interactions have been used in fully microscopic calculations of proton–light nuclei (nonlocal) effective interactions from which predictions of the elastic scattering differential cross sections and analysing powers have been obtained. Results for incident proton energies of 65 and 200 MeV are considered in particular herein. The associated relative motion wave functions have been used as the distorted waves in distorted wave approximation (DWA) studies of select inelastic scattering events. The same effective interactions were used as the transition operators in those calculations. The relevant nuclear spectroscopy for the elastic and DWA (p, p') calculations has been found from full $(0+2)\hbar\omega$ shell model evaluations of the nuclear structure; wave functions of which give good descriptions of form factors obtained from electron scattering.

1. Introduction

Understanding the nature and specifics of the potential energy of interaction between two colliding nuclei is central in almost all studies of their possible reactions. It remains so now that (secondary) radioactive beams can be produced and used to study collisions and structure of systems off the stability line with the results having relevance, for example, to modern studies of stellar processes.

Conventionally, elastic scattering data have been used as the measure of the candidate form of any such (nonrelativistic) interaction and it has long been a goal to ascertain that interaction with a proper direct approach in which underlying NN g matrices are folded with the density matrix elements of the colliding systems. The optical potential so defined is then nonlocal due to proper antisymmetrisation of the projectile and target nucleons, and to any nonlocality in the actual form for the chosen g matrices. The study of proton scattering from nuclei (or the equivalent, inverse kinematic scattering of nuclei from protons) is then favoured with such an approach as the antisymmetrisation is least problematic in the theoretical development of the optical potential. That is also the case for inelastic scattering when scattering amplitudes are specified

* Refereed paper based on a contribution to the Japan–Australia Workshop on Quarks, Hadrons and Nuclei held at the Institute for Theoretical Physics, University of Adelaide, in November 1995.

10.1071/PH96027 0004-9506/97/010245$05.00

in the DWA with appropriate, large basis space spectroscopy specifying the one body density matrix elements (OBDME) of each transition considered. The g matrices used to specify the nonlocal optical potentials should also be used as the transition operator effecting the inelastic events. But, to date, there have been few calculations made using such a stringent specification of a fully microscopic description of nucleon–nucleus (NA) scattering.

2. The NN t and g Matrices

A realistic microscopic model of NA reactions is one that is based upon realistic NN t matrices fully off the energy shell; i.e. with $E = k^2$ and in each channel $\alpha \equiv \{L', L, J, S, T\}$, we seek solutions of

$$t^{JST(+)}_{L'L}(p', p; E) = V^{JST}_{L'L}(p', p) + \frac{2}{\pi} \sum_{\ell} \lim_{\eta \to 0} \int V^{JST}_{L'\ell}(p', q) \left(\frac{1}{k^2 - q^2 + i\eta} \right) t^{JST(+)}_{\ell L}(q, p; E)\, q^2\, dq\,. \tag{1}$$

Input to these equations are the NN interactions, $(V^{JST}_{L'L}(p', p))$, which should be chosen from one of the 'realistic' set in the literature [1]. For convenience, in most of our studies we have used the Paris interaction. Contour plots of full-off-shell values of the t matrices have been published [2], as have the Kowalski–Noyes f-ratios which emphasise the half-off-shell properties.

But if the struck nucleon is embedded in a nuclear medium, then theoretical calculations of the NA optical potential, for example, should be based upon appropriate, medium modified NN g matrices, which are solutions of the BBG equations

$$g^{JST}_{L'L}(p', p; k, k_f) = V^{JST}_{L'L}(p', p) + \frac{2}{\pi} \sum_{\ell} \lim_{\eta \to 0} \int_0^{\infty} V^{JST}_{L'\ell}(p', q) \left[\frac{\bar{Q}(q, K; k_f)}{\bar{E}(q, K; k_f) - \bar{E}(k, K; k_f) + i\eta} \right] g^{JST}_{\ell L}(q, p; k, k_f)\, q^2 dq, \tag{2}$$

wherein $\bar{Q}(q, K; k_f)$ is the (angle averaged) Pauli operator and K is the average centre of mass momentum as defined previously [3, 4], with the latter specified at a laboratory incident momentum p_0 and for a Fermi momentum k_f. The energies in the propagators of the BBG equations include (real) auxiliary potentials U, and are defined by

$$\bar{E}(q, K; k_f) = (q^2 + K^2) + U(|\mathbf{q} + \mathbf{K}|) + U(|\mathbf{q} - \mathbf{K}|)\,. \tag{3}$$

Details of the calculations have been given previously [4] and the result is tables of complex numbers for each incident energy, Fermi momentum value and set of relative momenta for each NN channel. In a free NN collision the struck nucleon initially has zero momentum. Now, as it is embedded in (local) nuclear matter, that struck nucleon can have a range of momentum values; the major effect of which is to vary the on-shell values from those of free NN scattering [4].

3. Effective NN Interaction

The tables of g matrix elements are the input database for an effective interaction parametrisation scheme [5]. Specifically we have selected the half-off-shell t and g matrix elements in the procedure to find an optimum effective interaction which, in coordinate space, has the form

$$g_{eff}^{(i)ST}(r, E; k_f) = \sum_{j=1}^{n_i} S_j^{(i)}(E; k_f) \frac{e^{-\mu_j^{(i)} r}}{r} \,. \tag{4}$$

This form is used in the optical potential and DWA calculations performed by the computer program DWBA91 [6] where the index identifies the central force $\{\mathbb{I}\,, (\sigma \cdot \sigma)\,, (\tau \cdot \tau)\,, (\sigma \cdot \sigma)(\tau \cdot \tau)\}$, the tensor force $\{\mathbf{S}_{12}\}$ and the two body spin–orbit force $\{\mathbf{L} \cdot \mathbf{S}\}$. In this specification, $S_j^{(i)}(E; k_f)$ are complex, energy and density $(k_f(r))$ dependent strengths.

Across a large energy spectrum (to 800 MeV protons), we have selected the inverse ranges μ_i to be independent of both the energy and density. Specifically, values of $0{\cdot}71$, $1{\cdot}758$, $2{\cdot}949$ and $4{\cdot}0\,\mathrm{fm}^{-1}$ have been used for the central components and $1{\cdot}25$, $2{\cdot}184$, $3{\cdot}141$ and $4{\cdot}0\,\mathrm{fm}^{-1}$ for both the tensor and two body spin–orbit attributes. Excellent reproduction of the NN g matrices has been found, although the system of equations in the mapping scheme is grossly overdetermined so that other possible 'optimal' sets of parameters exist. But the key factor which we have stressed is that the resultant effective interaction chosen must be a good representation of the NN (t and) g matrices central in a microscopic theory of the optical potential. Effective interactions have been found in that way for protons (on light nuclei to ^{16}O) with energies in the range 60 to 800 MeV [7]. This has not been the case generally with other effective interactions, especially those predicated upon fitting many nucleon data.

4. A Fully Microscopic Model of Elastic and Inelastic Proton Scattering

To date there have been few calculations made using a fully microscopic description of NA scattering as stringent as that given in the Introduction. To do so one must have very good specifications of three primary ingredients. First, one must make a large basis space calculation of the structure of the target and its excited states, from which one obtains the individual state density distributions (needed to specify the optical potentials) and the OBDME, $S_{j_1 j_2 I}^{J_i J_f} = \langle \Psi_{J_f} || \, [a_{j_2}^\dagger \times a_{j_1}]^I \, || \Psi_{J_i} \rangle$. These we have obtained by making full $(0+2)\hbar\omega$ shell model calculations of the structure of various light nuclei. The single nucleon wave functions are the second ingredient in these studies. For the bound states we have used either harmonic oscillator or Woods–Saxon functions; the parametric values for which have been set, wherever possible, from analyses of elastic electron scattering form factors. They are not varied thereafter. The continuum (distorted) wave functions were obtained from the nonlocal optical potentials formed by folding the third ingredient, the effective NN interaction as discussed above, with the target state density matrices. The nonlocalities of the optical potentials arise in part as we properly antisymmetrise the total $(A+1)$ state wave functions. The resultant (fully microscopic) spin dependent, nonlocal forms for the optical potentials have been used in the Schrödinger equation, the solution of which enabled us to predict differential cross sections and analysing

powers for elastic scattering of protons from various light nuclei. The scattering waves obtained from these nonlocal interactions were then used as the distorted wave functions in DWA analyses of various inelastic scattering cross sections and analysing powers. The same effective interactions were used therein as the transition operators. In all cases, with both the elastic and inelastic transitions, a single calculation has been made from which the results are compared with the data. No scaling or variation of details has been made to 'improve' the comparisons that will be shown later.

(4a) Some Details of the Calculations

The spectrum and OBDME for $^{6,7,9,11}Li$, ^{12}C, ^{14}N and ^{16}O have been calculated using the code OXBASH [8] and a standard MK3W force [9]. The spectrum of ^{12}C so obtained up to 20 MeV excitation energy has been displayed and discussed in some detail [10]. With the exception of the known strongly deformed states [the $3^-;0(9{\cdot}64\,\mathrm{MeV})$ and $0^+;0(7{\cdot}65\,\mathrm{MeV})$ states], our spectrum agrees with observation to better than an MeV for all states up to 20 MeV excitation. From that spectrum, the OBDME for all transitions have been found to facilitate a complete analysis of electron scattering form factors, longitudinal and transverse, from which excellent agreement with observation was found, by and large, especially when meson exchange current effects are taken into account [11].

(4b) The Optical Potentials and Elastic Scattering

With the chosen form of the effective interaction folded with the target density matrices and upon antisymmetrising the NA wave function, a complex nonlocal spin dependent optical potential results in the form

$$\begin{aligned} U(\vec{r}_1,\vec{r}_2;E) &= \delta(\vec{r}_1-\vec{r}_2)\sum_n \zeta_n \int \varphi_n^*(\vec{s})v^D(\vec{r}_{1s},E;\rho[k_f(s)])\varphi_n(\vec{s})\,d\vec{s} \\ &\quad + \sum_n \zeta_n\varphi_n^*(\vec{r}_1)v^{Ex}(\vec{r}_{12},E;\rho[k_f(r_2)])\varphi_n(\vec{r}_2) \\ &\Rightarrow U_D(\vec{r}_1,E)+U_{Ex}(\vec{r}_1,\vec{r}_2;E)\,, \end{aligned} \tag{5}$$

wherein v^D and v^{Ex} are appropriate combinations of the NN ST channel elements of the effective interaction, $\varphi_j(\vec{r})$ are the single nucleon bound state wave functions and ζ_n are the shell occupancies of the target nucleus. The leading term has been used alone in the past, or the nonlocal (exchange) elements have been approximated by 'equivalent' local interactions. Neither is a satisfactory approach for the analyses of data from the scattering of intermediate energy protons (200 MeV herein) let alone the results for 65 MeV protons.

Results for the elastic scattering of 200 MeV protons from ^{12}C are presented in Fig. 1. The solid and dashed curves shown were obtained by using Woods–Saxon and harmonic oscillator (HO) wave functions respectively and the results shown in the left panels were obtained using our effective interactions but with the restriction that they are only those mapping the free NN t matrices (i.e. $k_f = 0$). It is evident that the medium modifications are essential to give a good fit to the data, especially the analysing power. We have also analysed the elastic scattering data from many other nuclei in this energy region including that of 160 MeV

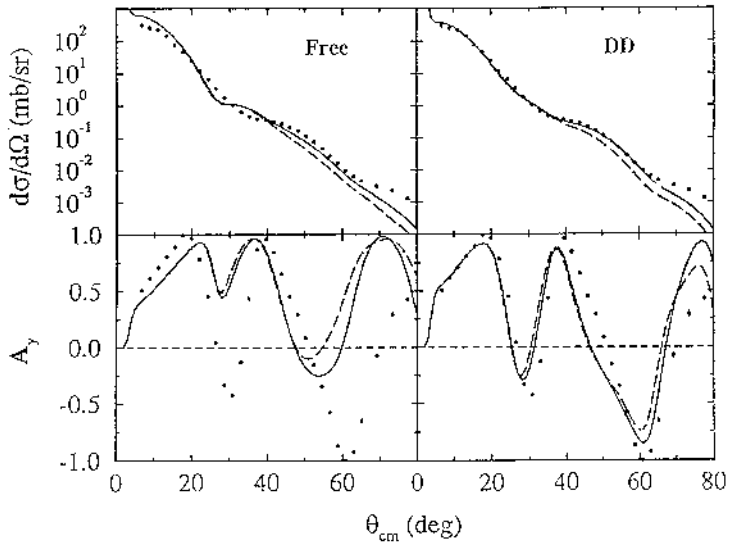

Fig. 1. The 200 MeV proton elastic scattering cross section and analysing power data compared with the results found using the (nonlocal) microscopic optical potentials built using the free NN t matrices (left) and the full interaction (right).

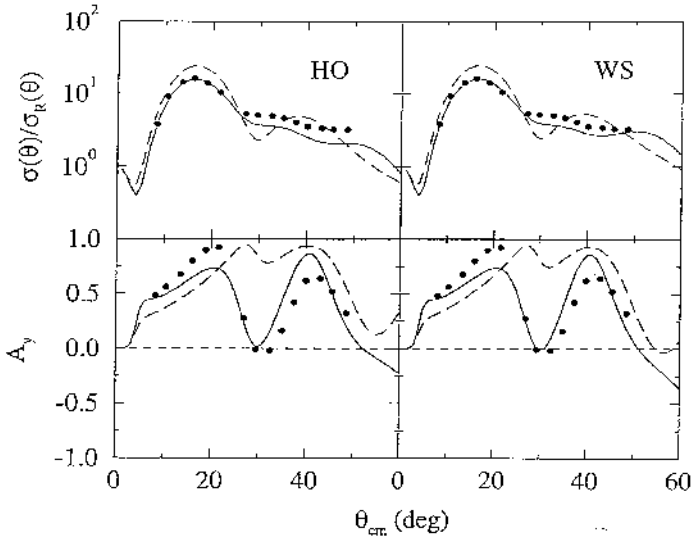

Fig. 2. Differential cross section and analysing power for the elastic scattering of 160 MeV protons from ^{14}N.

protons from ^{14}N, the results of which are given in Fig. 2. In this case the results found using WS and HO functions are shown in the right and left panels respectively, while the solid and dashed curves display the results we have obtained using our effective interaction (based at 160 MeV) throughout and the density dependent Love–Franey (LF) force [12] respectively. The results found with our

force compare much more favourably with the data, especially the analysing power

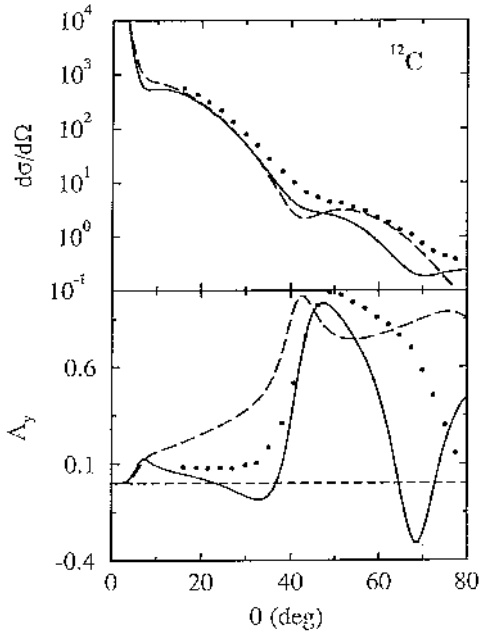

Fig. 3. Differential cross section and analysing power for the elastic scattering of 65 MeV protons from ^{12}C.

At 65 MeV, the results of our calculations are not in as good agreement with data as are those at 200 MeV. The deficiency lies mainly with the current specification of the 65 MeV NN g matrices, and with the average potentials that enter the energy propagators in particular. However, despite the lack of total strength required, there are signatures of medium effects in data that indicate a propriety in form of the present effective interaction. As we shall demonstrate, with but a small scale enhancement, we have a good model effective interaction. The cross section and analysing power for the elastic scattering of 65 MeV protons from ^{12}C are displayed in Fig. 3. The data are compared with the results obtained by folding the effective interactions found from the free t matrices (dashed curves) and from the mapping of the NN g matrices (solid curves). Clearly our (65 MeV) interaction is too weak as both cross sections lie below the data at the larger scattering angles. But the medium modifications give a mix of operator terms that lead to the observed shape of the measured analysing power. Likewise, and as displayed in Fig. 4, the cross section from the elastic scattering of 65 MeV protons from ^7Li is underpredicted by calculation, whether made using the free or the medium modified effective interactions. The analysing powers of the two calculations are again noticeably different with the calculations made using the effective interaction built upon the NN g matrices again giving the better agreement with experiment. Finally, so far as the elastic scattering study is concerned, we show in Fig. 5 the differential cross sections found recently from the elastic scattering of 60 MeV/A ^9Li and of 62 MeV/A ^{11}Li ions from protons. The results displayed were obtained using the medium modified effective interaction, Woods–Saxon bound state wave functions and $(0+2)\hbar\omega$ spectroscopy. The ^9Li calculated result underpredicts the data as was the case for the ^7Li scattering, but the result for the 'halo' nucleus ^{11}Li is

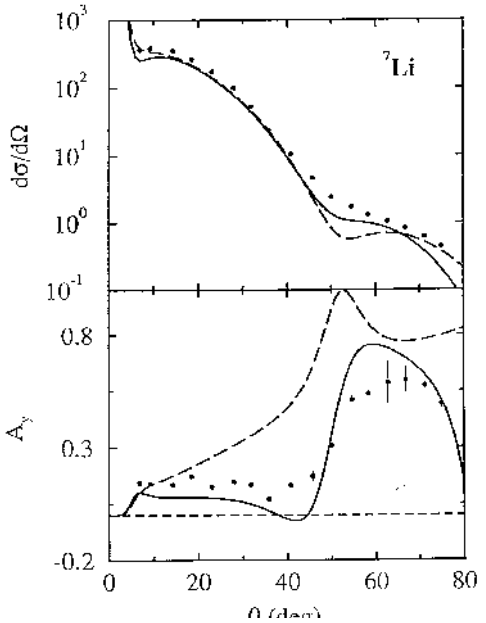

Fig. 4. Differential cross section and analysing power for the elastic scattering of 65 MeV protons from ^7Li.

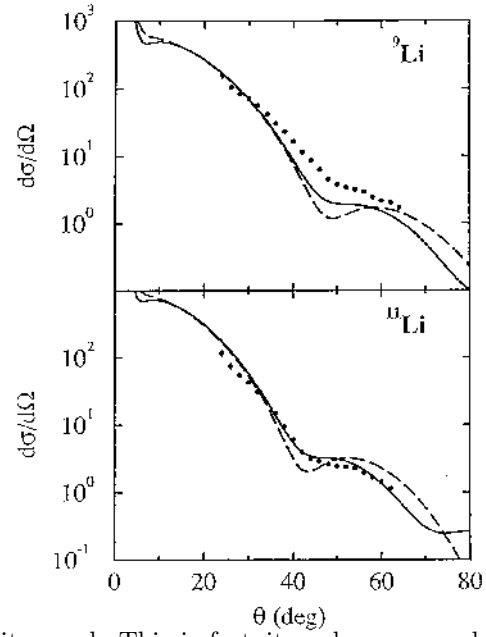

Fig. 5. Differential cross sections for the elastic scattering of 60 MeV/A ^9Li and 62 MeV/A ^{11}Li ions from protons.

quite good. This is fortuitous however and we expect that to retain such a good fit when a proper effective interaction for this energy regime has been defined, we may need to have a quite different matter distribution for ^{11}Li, i.e. much more of a 'halo' than the current spectroscopy suggests.

(4c) DWA Analyses of Inelastic Scattering

In the DWA, transition amplitudes take the form

$$T_{J_i,J_f}(\theta) = \langle \chi^{(-)}(\vec{k}_f,0)|\langle \Psi_{J_f}(1\cdots A)|\, Av_{eff}(0,1)\, \mathcal{A}_{01}\{|\chi^{(+)}(\vec{k}_i,0\rangle|\Psi_{J_i}(1\cdots A)\rangle\}\,, \quad (6)$$

where the distorted waves are denoted by $|\chi^{(\pm)}\rangle$ and $\mathcal{A}_{01}$ is an antisymmetrisation operator. By using a cofactor expansion of the A–nucleon wave functions, the dependence upon coordinate '1' can be isolated so that

$$T_{J_i,J_f}(\theta) = \sum_{(j_1 j_2)} \langle \Psi_{J_f} | a^{\dagger}_{(j_1)} \times a_{(j_1)} | \Psi_{J_i} \rangle \times \langle \chi^{(-)}(0) | \langle \varphi_{j_2}(1) |\, v_{eff}(01)\, \mathcal{A}_{01} \{ |\chi^{(+)}(0)\rangle | \varphi_{j_1}(1) \rangle \} \,. \tag{7}$$

The Wigner–Eckart theorem then relates the multi-nucleon aspects of these transition amplitudes to the OBDME one obtains from structure calculations. More details are given in ref. [9].

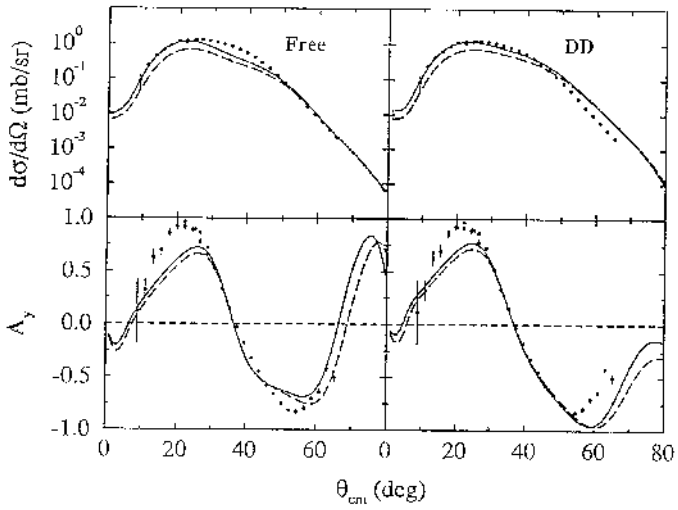

Fig. 6. Differential cross section and analysing power from the inelastic scattering of 200 MeV protons from ^{12}C leading to the $2^+_1;0$ (4·44 MeV) state. The data are compared with the results of our DWA calculations made using the microscopic optical model interactions for the free and density dependent interactions (left and right panels) and the $(0+2)\hbar\omega$ and CK ($0p$) models of spectroscopy (solid and dashed curves).

In Fig. 6 the results of our DWA calculations for the cross sections and analysing powers from 200 MeV protons on ^{12}C and exciting the $2^+_1;0$ (4·44 MeV) state are compared with the data. With both the free and density modified effective interactions, the larger basis structure calculations increase the predicted magnitudes above those found using the CK wave functions and bring them into quite good agreement with measurement. The results reflect the similar effects noted when those same structure functions were used in calculations of electron scattering form factors. The medium modified effective interaction leads to very good results (in comparison with the data) reproducing the shape and magnitude of cross section data to 50°. The analysing powers are likewise better reproduced by the medium modified effective interaction calculations. Recall that the effective interaction has been used to define the optical potentials (initial and

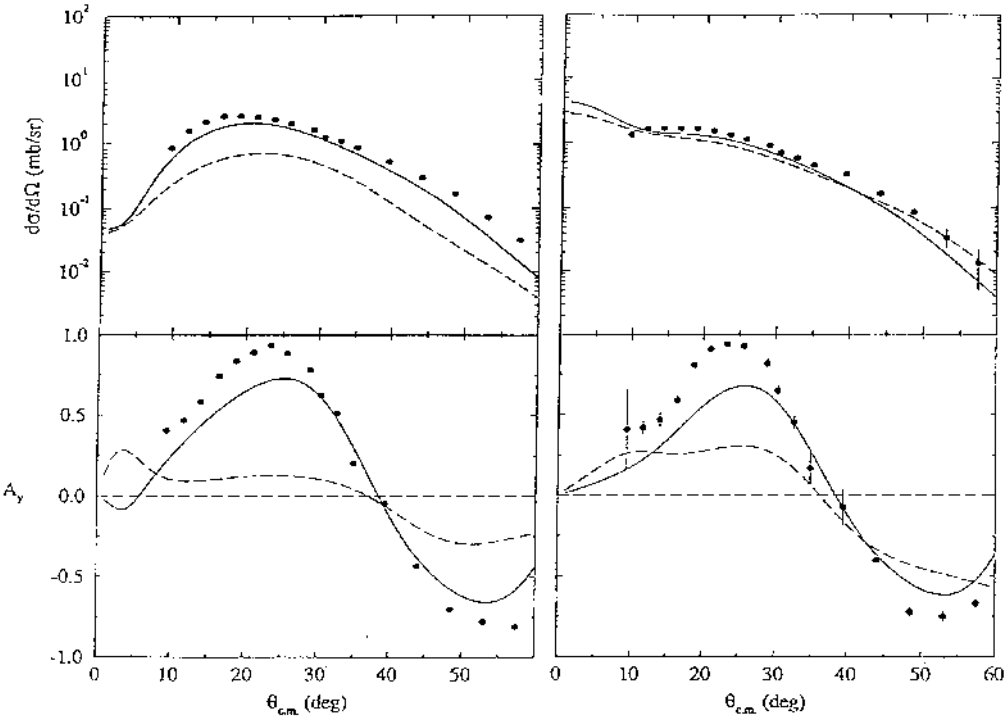

Fig. 7. Differential cross sections (top) and analysing powers (bottom) for the inelastic scattering of 200 MeV protons from ^7Li leading to the $\frac{1}{2}^-$ state at 0·478 MeV excitation (left panel) and to the $\frac{7}{2}^-$ state at 4·63 MeV excitation (right panel). The results found using the $0\hbar\omega$ and $(0+2)\hbar\omega$ structures are displayed by the dashed and solid curves respectively.

final channels) in these DWA calculations and we stress again that *no* arbitrary scaling has been used nor have the bound state wave functions been adjusted seeking better fits to data. Similarly good results have been found with a number of other transitions in ^{12}C, not only at 200 MeV but also for energies up to 800 MeV [9].

Finally, we display results from calculations of the differential cross sections and analysing powers from the inelastic scattering of 200 MeV protons from ^7Li. In Fig. 7 the data from the excitation of the $\frac{1}{2}^-$, (0·478 MeV) and $\frac{7}{2}^-$, (4·63 MeV) states are compared in the left and right panels respectively, with the results of calculations made using Woods–Saxon bound state wave functions and our density dependent effective interaction. The differential cross sections and analysing powers are shown in the top and bottom segments respectively. Two sets of OBDME, from the $0\hbar\omega$ and $(0+2)\hbar\omega$ spectroscopies, were used to obtain the results displayed by the dashed and solid curves respectively. These results clearly demonstrate that a large basis spectroscopy is required to understand the observations with the $\frac{7}{2}^-$ state excitation at least. Not only are the shape and magnitude of that differential cross section much better reproduced but so also, and more dramatically, are those of the analysing power. The analysing power prediction for the $\frac{1}{2}^-$ excitation shows the need for a large basis spectroscopy in

that case. The major effect of the extended basis is to enhance the E2 character of the transitions; notably in the cross sections of the $\frac{7}{2}^-$ case.

5. Conclusions

Fully microscopic model calculations of elastic and (select) inelastic scattering data taken with incident protons at energies of 200 and 65 MeV have been made. Both differential cross section and analysing power data have been analysed. The elastic scattering data have been analysed by forming optical potentials via folding effective NN interactions with the density matrices of the ground states of various light nuclei. The results are complex, nonlocal potentials with which good to excellent fits were found to both the elastic cross sections and analysing powers, although there remains a need to improve the details of the effective NN interactions, especially 65 MeV.

The same NN effective interactions were used as the transition operators in a DWA study of various inelastic scatterings wherein the distorted waves were found consistently by folding the interactions with the initial and final state density matrices. With OBDME given by large basis shell model calculations, the cross sections and analysing powers for those transitions to discrete excited states have been fit very well.

References

[1] M. Lacombe, B. Loiseau, J. M. Richard, R. Vinh Mau, J. Côté, P. Pirès and R. de Tourreil, Phys. Rev. **C21** (1980) 861; R. Machleidt, K. Holinde and Ch. Elster, Phys. Rep. **149** (1987) 1; V. G. J. Stoks, R. A. M. Klomp, C. P .F. Terheggen and J. J. de Swart, Phys. Rev. **C49** (1994) 2950.
[2] K. Amos, L. Berge, F. A. Brieva, A. Katsogiannis, L. Petris and L. Rikus, Phys. Rev. **C37** (1988) 934.
[3] M. I. Haftel and F. Tabakin, Nucl. Phys. **A158** (1970) 1.
[4] P. J. Dortmans and K. Amos, J. Phys. **G17** (1991) 901.
[5] H. V. von Geramb, K. Amos, L. Berge, S. Bráutigam, H. Kohlhoff and A. Ingermarsson, Phys. Rev. **C44** (1991) 73.
[6] J. Raynal, computer program DWBA91 (NEA 1209/02).
[7] P. J. Dortmans and K. Amos, University of Melbourne Reports UM-P-95/27 and UM-P-95/41 (1995), unpublished.
[8] OXBASH–MSU (the Oxford–Buenos-Aries–Michigan State University shell model code). A. Etchegoyen, W. D. M. Rae and N. S. Godwin (MSU version by B. A. Brown); B. A. Brown, A. Etchegoyen and W. D. M. Rae, MSUCL Report No. 524 (1986).
[9] S. Karataglidis, P. J. Dortmans, K. Amos and R. de Swiniarski, Phys. Rev. **C52** (1995) 861; *ibid.* **53** (1996) 838; Aust. J. Phys. **49** (1996) 645; P. J. Dortmans, S. Karataglidis, K. Amos and R. de Swiniarski, Phys. Rev. **C52** (1995) 3224.
[10] S. Karataglidis, University of Melbourne Report UM-P-95/29 (1995).
[11] S. Karataglidis, P. Halse and K. Amos, Phys. Rev. **C51** (1995) 2494.
[12] M. A. Franey and W. G. Love, Phys. Rev. **C31** (1985) 488.